Available online at www.sciencedirect.com

ScienceDirect

Proceedings of the Combustion Institute 35 (2015) 1451–1459

Proceedings of the Combustion Institute

www.elsevier.com/locate/proci

Experimental investigation of Darrieus–Landau instability effects on turbulent premixed flames

G. Troiani [a], F. Creta [b,*], M. Matalon [c]

[a] ENEA C.R. Casaccia, via Anguillarese 301, Rome, Italy

[b] Dept. of Mechanical and Aerospace Engineering, University of Rome "La Sapienza", Rome, Italy

[c] Dept. of Mechanical Science and Engineering, University of Illinois at Urbana-Champaign, Urbana, IL 61801, USA

Available online 15 August 2014

Abstract

The turbulent propagation speed of a premixed flame can be significantly enhanced by the onset of Darrieus–Landau (DL) instability within the wrinkled and corrugated flamelet regimes of turbulent combustion. Previous studies have revealed the existence of clearly distinct regimes of turbulent propagation, depending on the presence of DL instabilities or lack thereof, named here as super- and subcritical respectively, characterized by different scaling laws for the turbulent flame speed.

In this study we present experimental turbulent flame speed measurements for propane/air mixtures at atmospheric pressure, variable equivalence ratio at Lewis numbers greater than one obtained within a Bunsen geometry with particle image velocimetry diagnostics. By varying the equivalence ratio we act on the cut-off wavelength and can thus control DL instability. A classification of observed flames into sub/supercritical regimes is achieved through the characterization of their morphology in terms of flame curvature statistics. Numerical low-Mach number simulations of weakly turbulent two-dimensional methane/air slot burner flames are also performed both in the presence or absence of DL instability and are observed to exhibit similar morphological properties.

We show that experimental normalized turbulent propane flame speeds S_T/S_L are subject to two distinct scaling laws, as a function of the normalized turbulence intensity U_{rms}/S_L, depending on the sub/supercritical nature of the propagation regime. We also conjecture, based on the experimental results, that at higher values of turbulence intensity a transition occurs whereby the effects of DL instability become shadowed by the dominant effect of turbulence.

Keywords: Premixed turbulent flames; Bunsen flames; Darrieus–Landau instability; Turbulent propagation speed; Flame curvature

1. Introduction

The search for a universal scaling law for the turbulent propagation speed of premixed flames is still debated and systematically complicated by the wide scatter of experimental results, often

* Corresponding author.

E-mail addresses: guido.troiani@enea.it (G. Troiani), francesco.creta@uniroma1.it (F. Creta), matalon@illinois.edu (M. Matalon).

http://dx.doi.org/10.1016/j.proci.2014.07.060

1540-7489/

due to the strong dependence from experimental conditions [1–3], and by a general disagreement with proposed theories.

In the context of flame–turbulence interaction, the presence of intrinsic Darrieus–Landau (DL) hydrodynamic instabilities, especially when the incident turbulence is weak, were recognized as an important factor influencing the propagating characteristics of flames [4–6]. A number of experimental studies were performed [7–13] with emphasis on the role of DL instability. Although no final quantitative agreement yet exists on such role [1], there is mounting evidence that the bifurcative transition to DL instability greatly influences turbulent flame morphology and dynamics, hinting at the existence of a multiplicity of scaling laws for the turbulent propagation speed.

In a laminar scenario [14,15] a planar flame transitions, upon onset of DL instability, to a typical large scale cusp-like corrugated conformation steadily propagating at a speed substantially greater than the unstretched laminar flame speed S_L. Recently, in a series of numerical studies by Creta and Matalon [16–19], it was found that in a turbulent scenario a similar dichotomy persists. Thus, an originally laminar and stable planar flame will remain statistically planar, defining a *subcritical* turbulent mode (or regime) of propagation, whereas an unstable flame in the presence of turbulence will exhibit a more complex corrugation, with sharp cusps protruding into the burnt mixture, hence defining a *supercritical* turbulent mode in which DL effects are dominant. For each mode of propagation, such studies highlighted the presence of clearly distinct scaling laws for the turbulent speed S_T, expressed in the form $S_T/S_L \sim (U_{rms}/S_L)^n$, with U_{rms} the intensity of the turbulent field in terms of the r.m.s. of velocity fluctuations. In particular, indicating the two modes with subscripts *sub, sup* it was observed that (*i*) $(S_T/S_L)_{sup} > (S_T/S_L)_{sub}$ owing to increased flame corrugation leading to a DL-enhancement of the turbulent speed, (*ii*) scaling exponents are subject to $n_{sup} < n_{sub}$ indicating that the supercritical mode is less sensitive to turbulence, and (*iii*) DL effects are overpowered by the increasing wrinkling at high turbulent intensities, with the scaling exponent n reverting back to values similar to subcritical behavior.

A rather similar scenario was recently proposed by Chaudhuri [20] where a limiting condition was identified at which turbulence suppresses the effects of DL instability. If, however, DL instabilities can develop in weaker turbulence, then two distinct scaling laws for the turbulence speed, derived through spectral closure techniques and self similarity arguments, indeed emerge.

In this work we present experimental evidence for the above general dual behavior for turbulent flame speed, induced by the presence or absence of intrinsic DL instabilities. We adopt a $D = 18$ mm diameter propane–air Bunsen flame at atmospheric pressure and variable equivalence ratio ϕ and variable inflow turbulence intensity equipped with particle image velocimetry (PIV) diagnostics. Results are supported by two dimensional low-Mach number direct numerical simulations of methane–air turbulent Bunsen flames, performed to investigate the morphological differences between subcritical and supercritical modes of propagation.

2. Determination of stability limits

We defined super/subcritical turbulent regimes as flame propagation modes characterized respectively by the presence or absence of DL instability. Figure 1 displays Mie scattering images of propane–air Bunsen flames, subject of the present investigation, qualitatively illustrating the morphological differences of such propagative modes. We note smooth convex/concave wrinkling in the subcritical regime as opposed to sharp cusp-like protrusions towards the burnt mixture typical of DL corrugation which characterizes the supercritical regime. A general guideline is thus needed to discriminate between such regimes and possibly control their onset as a function of the independent parameters available in the context of an experimental setting.

Given a characteristic hydrodynamic length L, representative of the transverse dimension of the flame or device producing it, a planar laminar flame can become unstable to disturbances of long wavelength λ if stabilizing effects, of thermal diffusive nature, are insufficient to the extent of decreasing the critical (cut-off) disturbance wavelength λ_c below L so that $\lambda_c < \lambda < L$. Increasing the pressure or driving the mixture composition towards stoichiometric conditions can indeed reduce the flame thickness and thus the Markstein length, which is of the same order, and which in turn decreases λ_c thus promoting instabilities. In the context of the hydrodynamic theory of premixed flames the linear stability analysis of a planar flame yields asymptotic dispersion relations [21–23] in the form of truncated series expansions in powers of the transverse wavenumber $k = 2\pi/\lambda$, expressing the disturbance growth rate $\omega(k)$. As shown in [14], simplified Markstein-type flame models can yield a closed form dispersion relation yielding similar qualitative results. Such models generally retain corrective diffusive effects only in the flame speed expression $S_f = S_L - \mathscr{L}\mathbb{K}$, where S_f is defined as the speed relative to the unburnt mixture and where $\mathscr{L}$ is the Markstein length and $\mathbb{K}$ is the flame stretch. The closed form dispersion relation yields a cut-off disturbance wavelength, defined at $\omega = 0$ (see bold continuous and dashed lines in Fig. 2), which

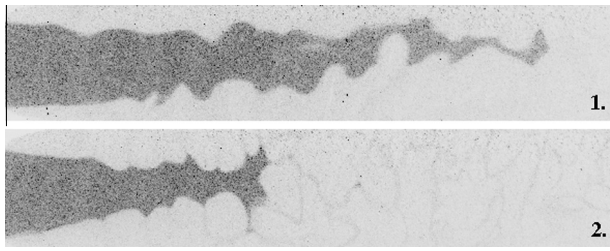

Fig. 1. Mie scattering images (rotated 90°) of propane–air Bunsen flames at atmospheric pressure and $Re = 5000$. 1. Subcritical regime, $\phi = 0.8$;; 2. Supercritical regime, $\phi = 1.4$.

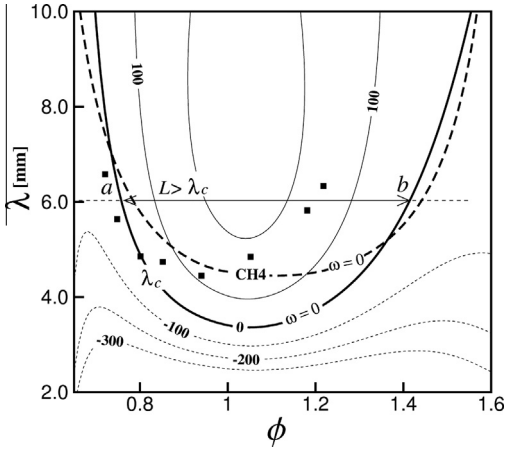

Fig. 2. Growth rate $\omega(\lambda, \phi)$ for a propane–air planar flame at atmospheric pressure. Continuous lines: $\omega = \text{const.} > 0$ (unstable planar flame), dotted lines: $\omega = \text{const.} < 0$ (stable planar flame). Bold continuous line: cut-off wavelength λ_c defined as $\omega(\lambda_c, \phi) = 0$ for propane–air mixtures. Bold dashed line: cut-off wavelength for methane–air mixtures. Filled symbols: experimentally derived λ_c values for propane–air V-flames [27].

is found to be $\lambda_c = 2\pi(3\sigma - 1)\mathscr{L}/(\sigma - 1)$ where $\sigma = \rho_u/\rho_b$ is the unburnt to burnt gas density ratio. This can be related to the equivalence ratio ϕ by determining the functions $\mathscr{L}(\phi)$ and $\sigma(\phi)$ for propane–air mixtures. The generalized hydrodynamic theory provides a comprehensive expression for the Markstein length in terms of functional parameters that can be extracted by experimental data which reads

$$\mathscr{L}/\delta_D = \frac{\sigma}{\sigma - 1}\int_1^\sigma \frac{\eta(\tau)}{\tau}d\tau + \frac{Ze(Le_{\text{eff}} - 1)}{2(\sigma - 1)} \times \int_1^\sigma \frac{\eta(\tau)}{\tau}\ln\left(\frac{\sigma - 1}{\tau - 1}\right)d\tau \quad (1)$$

where the diffusion length scale $\delta_D = D_{th}/S_L$ is a measure of the laminar flame thickness, with D_{th} taken as the thermal diffusivity, Ze the Zel'dovich number, $\eta(T/T_u)$ summarizes the temperature dependence on transport and Le_{eff} is a weighted average of the fuel and oxidizer Lewis numbers (details in [24,25]).

Figure 2 is a plot of the perturbation growth rate $\omega(\lambda, \phi)$ obtained using the closed form asymptotic dispersion relation [14] for a planar flame, inclusive of Eq. (1) and adopting experimental data by Tseng et al. [26] for propane mixtures at atmospheric pressure which was fitted to establish the dependence of all functional parameters from ϕ. We find that for such mixtures $\mathscr{L}(\phi) > 0$, corresponding to large Le_{eff}, ranging from 1.8 to 1.35 in the interval $\phi \in [0.6, 1.6]$, which excludes the possibility of thermal diffusive instabilities. Figure 2 shows that given a fixed hydrodynamic length L, representative of the lateral domain size, the condition $L > \lambda_c$ defines an island of instability in terms of flame composition roughly centered at $\phi = 1$. In other words when $\phi \in [\phi_a, \phi_b]$ the growth rate $\omega > 0$ for all disturbances of wavelength $\lambda_c < \lambda < L$, thus promoting DL instability. Experimental points in Fig. 2, obtained by harmonically forcing a premixed flame [27], confirm the existence of such an instability ϕ-interval albeit for a rod-stabilized V-flame configuration. We note that in the linear regime, any small disturbance on the planar flame grows exponentially in amplitude but is eventually stabilized by nonlinear effects into a large-scale, cusp-like conformation typical of DL instability.

Applying such reasoning to a Bunsen rather than a planar flame, the hydrodynamic length L may be assumed to be related to the nozzle diameter and to the outflow velocity, although some ambiguity persists on its exact determination and thus on the determination of the instability island, given the lack of a general theory. Inspection of Fig. 2 further suggests that for given operating conditions a minimum nozzle diameter exists below which DL instability is not expected at any ϕ.

3. CFD of Bunsen flames

The foregoing section established the general criterion, derived for a planar flame, that DL

instability, if present, will occur in a composition interval roughly centered about $\phi = 1$. Such criterion, when extended to atmospheric pressure Bunsen flames, thus proves only as a useful guideline in triggering a supercritical propagative mode from a subcritical one (such as those visible in Fig. 1) by driving a lean mixture towards a richer composition and vice versa, provided that for a given outflow velocity, L, which can be considered proportional to the Bunsen nozzle diameter, is large enough to guarantee a finite instability composition interval. Yet, the ambiguity on L and thus on the size of such interval makes the above guideline a necessary but not a sufficient condition for the existence of DL instability. In order to better distinguish supercritical configurations from subcritical an additional observable is needed.

In a mildly turbulent scenario, it was shown by Creta and Matalon in [18,19], through numerical simulations, that a supercritical flame exhibiting DL instability manifests a characteristic morphology due to the interaction of turbulence with the cusp-like structures appearing on its surface and protruding towards the combustion products. In particular, such interaction was shown to induce asymmetric flame curvature probability density functions (p.d.f.), skewed towards negative curvatures while a symmetric p.d.f. is generally observed for subcritical flames. Defining curvature as $\kappa = -\nabla \cdot \mathbf{n}$, where $\mathbf{n}$ is the unit normal at the flame surface pointing towards the burnt gases, a negative skewness of curvature distribution (defined as its third moment γ) is indicative of a flame being highly convex towards the burnt side and only mildly convex towards the fresh side. Such asymmetric morphological features were observed adopting both a weakly non linear model [19] and a hybrid front-capturing/Navier–Stokes model [18] of a planar flame assumed of vanishing thickness with respect to the smallest fluid scales. In both cases a linear stability theory exists in closed form yielding an unambiguous instability criterion defined by the cut-off condition $L > \lambda_c$, where L is uniquely defined as the lateral domain size. Thus, asymmetric curvature (as well as flame position) distributions could be linked directly to the presence of DL effects. In an experimental Bunsen setting, however, the skewness of flame curvature distribution, is only expected to be an efficient qualitative marker for the presence of DL instability. Still, we can infer that supercritical regimes will be more likely if characterized by highly skewed curvature p.d.f.'s and compositions close to stoichiometric, while subcritical regimes will be more likely to possess less skewed, if not symmetric p.d.f.'s and compositions far from stoichiometric.

In order to assess whether such morphological observations preserve their validity for flames of finite thickness in a Bunsen burner configuration, we perform direct numerical simulations using the full reactive Navier–Stokes equations. The simulations are carried out in a two-dimensional setting, effectively representing a slot rather than a Bunsen burner. As shown in [19], through a forced Michelson–Sivashinsky model, valid for $\sigma - 1 \ll 1$, two-dimensional flames preserve the same morphological and propagative features as three-dimensional flames in the context of the interaction of DL flame structures with turbulence.

The adopted numerical scheme is based on the unfiltered time-dependent low-Mach number equations with detailed chemistry and without buoyancy and radiation effects. An operator-split stiff second-order predictor–corrector projection scheme is employed, full details of which can be found in [28–30]. We choose a methane–air mixture described by a 16 species and 57 reactions chemical mechanism obtained via a Computational Singular Perturbation (CSP) simplification algorithm [31] starting from a detailed Gri1.2 mechanism. We employ a grid resolution of 45 μm which accommodates a minimum of 10 grid points within the flame thickness defined on the basis of the temperature profile. Burnt gases are fed externally of the fresh mixture nozzle outflow to stabilize the flame and to avoid Kelvin–Helmholtz shear instabilities. A weak isotropic turbulent field is fed through the mean fresh Bunsen outflow using a technique identical to that described in [18].

Two distinct simulations were performed, displayed in Fig. 3 at various time instants, effectively representing prototypical subcritical and supercritical configurations, which clearly exhibit a fundamentally distinct morphology. Flame (a) in Fig. 3 was obtained at atmospheric pressure for a nozzle diameter of 0.6 cm. A preliminary simulation of a spanwise periodic freely propagating laminar planar flame, of width $L = 0.6$ cm, exhibited stability when mildly perturbed at the same pressure level. This is indicative of the absence of DL instability in flame (a) which indeed exhibits subcritical features with a smooth flame surface wrinkling. The flame surface is defined without loss of generality as the 1200 K temperature isocontour and its curvature is displayed in the inset of Fig. 3, showing small positive/negative peaks hinting to a quasi symmetric curvature p.d.f., possibly moderately skewed towards negative values owing to the effect of the flame tip.

When the lateral domain is increased to $L = 1.2$ cm and the pressure raised to 2 atm, the preliminary simulation involving a mildly perturbed planar laminar flame was seen to exhibit instability with formation of DL cusps. As a result, flame (b) of Fig. 3, issuing from a nozzle diameter of 1.2 cm and appearing thinner due to the higher pressure, clearly exhibits permanent cusp-like structures due to DL instability typical of the supercritical regime. Such structures are

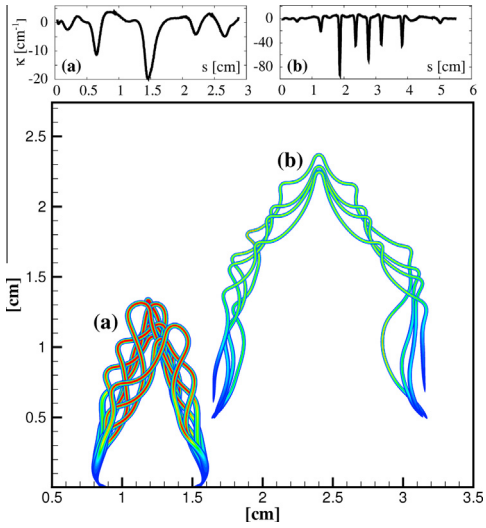

Fig. 3. Lower panel: two-dimensional simulation of stoichiometric methane–air slot flames. Shown is formyl (HCO) radical mass fraction ($Y_{HCO} < 10^{-6}$ not shown) at various time instants. (a) Subcritical flame at $p = 1$ atm, slot width $d = 0.6$ cm, (b) supercritical flame at $p = 2$ atm, $d = 1.2$ cm. Inflow turbulence $U_{rms}/S_L = 0.5$. Fresh mixture bulk velocity is taken as $\sqrt{10}S_L$ so that the laminar Bunsen flame height is $\sim 3/2d$. Upper panels: instantaneous flame curvature along the flame curve s at a representative time instant.

convected towards the tip, owing to the velocity component tangent to the flame, and their effect is to introduce sharp negative curvature peaks clearly visible in the inset of Fig. 3 which appear far larger in magnitude than in the subcritical case. We therefore conclude that the statistical characterization of flame curvature and in particular the skewness of its p.d.f. can act as an efficient marker for the onset of DL instability in an experimental Bunsen flame.

4. Experimental setup

As stated, sub/supercritical regimes are sought in a Bunsen flame in order to analyze their morphology and assess the influence of DL instability on turbulent flame speed. The Bunsen burner is operated at two different bulk Reynolds numbers and variable equivalence ratio. The use of 3 μm alumina particles dispersed into the flow guarantees unbiased probing of flow velocity across the flame front within the PIV setting [32,33]. The laser source is a 54 mJ Nd:YAG equipped with a 60 mm focal length camera working at a resolution of 1024×1280 pixels. The area recorded by CCD is 94.5×118.6 mm^2. Pulse to pulse delay is between 60 μs and 80 μs in order to attain a maximum particle displacement less than one-quarter of the interrogation window size (32×32 pixels) which presents 50% overlapping for velocity field estimation. Full details of the experimental setup may be found in [33–35].

The flame front position is determined from the sudden particle number density jump caused by the steep temperature increase in the reaction zone of premixed flames [36]. Within Mie scattering images this corresponds to zones at very different level of scattered light intensity. It follows that the locations with intensities higher than the threshold are defined as unburnt, i.e. the reaction progress variable c is set to zero and those with intensities lower than the threshold correspond to combustion products with $c = 1$. Successive averaging of a number of 400 binarized images yields the mean progress variable $\langle c \rangle$, whose value $\langle c \rangle = 0.5$ is set to be mean front position. Moreover, the turbulent intensity U_{rms} acting on the flame front from the reactant side is evaluated by taking the average of turbulent intensities conditioned to $\langle c \rangle = 0.02$. Once the average flame front position is defined, under the hypothesis of axisymmetricity of the mean field, the average surface area A_s is obtained and the turbulent speed follows from $S_T = \dot{m}/(\rho_u A_s)$.

From any single binarized image of the instantaneous flame front, the flame contour is extracted and a signed distance function ψ is evaluated with positive and negative values indicating products and reactants, respectively. The normal to the flame is constructed towards the products as $\mathbf{n} = \nabla\psi/|\nabla\psi|$ so that flame curvature can be established as stated in Section 3. Note that the largest absolute curvature that can be evaluated is limited physically by flame thickness (δ_D), which is of the order of 50–100 μm [26] and also by image resolution that in this case is 90 μm.

5. Results and discussion

Mie scattering images of Bunsen flames shown in Fig. 4 reveal a variable number density of cusp-like structures as a function of equivalence ratio. As an example, examination of flames ‘a’ and ‘I’, relative to lean mixtures, exhibit a clear subcritical morphology with flame wrinkling appearing almost equally convex as it is concave. On the other hand, flames ‘c’, ‘d’ and ‘III’, relative to richer mixtures, exhibit pointed structures protruding towards the burnt gases typical of the supercritical regime. Further increasing the equivalence ratio, flames seem to regain a subcritical morphology, as with flame ‘VI’ and ‘h’, through a decrease in the number of cusp-like structures.

As can be observed in Fig. 5, relative to the $Re = 2500$ case (flames I and III), these morphological observations, translate into flame curvature p.d.f.’s being skewed towards negative curvatures for supercritical flames.

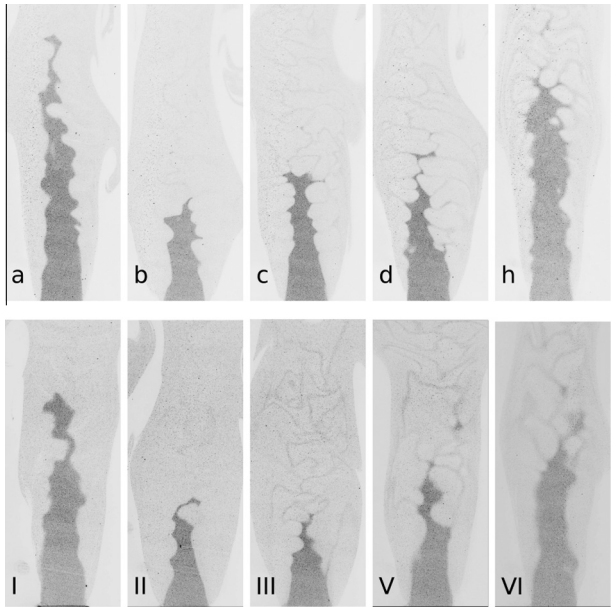

Fig. 4. Mie scattering images of C_3H_8/air flames at varying equivalence ratios (ϕ) and bulk Reynolds number, ($Re = 4\dot{m}/D\mu\pi$) with $\dot{m}$ mass flow rate. For the sake of clarity colors have been inverted so that dark zones correspond to reactants. Upper panels, $Re = 5000$: a, $\phi = 0.8$; b, $\phi = 1.1$; c, $\phi = 1.4$; d, $\phi = 1.5$; h, $\phi = 1.7$. Lower panels, $Re = 2500$: I, $\phi = 0.7$; II, $\phi = 0.9$; III, $\phi = 1.4$; V, $\phi = 1.6$; VI, $\phi = 1.7$. Flames e, $\phi = 1.55$, f, $\phi = 1.6$, g, $\phi = 1.65$ and IV, $\phi = 1.5$ not shown for brevity.

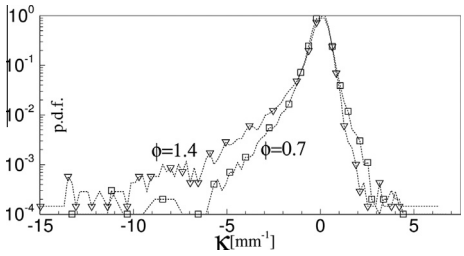

Fig. 5. Curvature p.d.f.'s for $Re = 2500$ flames. Squares: I, $\phi = 0.7$ (subcritical), triangles: III, $\phi = 1.4$ (supercritical).

The curvature analysis, in terms of p.d.f. skewness, was carried out on all performed experiments and is shown in Fig. 6 as a function of ϕ. We note higher absolute skewness for near stoichiometric values of ϕ, indicating likely presence of DL-type cusps, while smaller absolute values are attained for off stoichiometric compositions, hinting at a lower cusp number density. Also shown in Fig. 6 is the analytical linear stability criterion $L > \lambda_c$ for a planar propane flame, similarly to that shown in Fig. 2, clearly indicating the instability ϕ islands for a representative value of L. Although no threshold value for the skewness can be defined in this experimental setting, discriminating between sub- and supercritical flames,

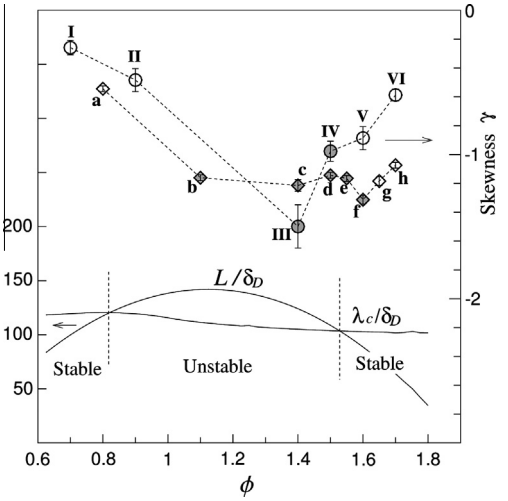

Fig. 6. Top curves: skewness of flame curvature p.d.f.'s. Circles: $Re = 2500$, diamonds: $Re = 5000$ (Experimental points labels correspond to Fig. 4 nomenclature). Error bars proportional to standard deviation of the measure (see [38] for details). Filled/empty symbols refer to scaling laws in Fig. 7. Bottom curves: representative hydrodynamic length L (taken as $L = 5$ mm) and cut-off wavelength λ_c for a planar flame, normalized with flame thickness δ_D. Expression of λ_c appearing in Section 2 was used.

similarly to the ambiguity existing on L, Fig. 6 clearly shows that in near-stoichiometric conditions (a necessary condition for DL instability) all flames exhibit highly skewed curvatures indicating a higher occurence of DL-type structures which define the supercritical regime.

An additional finding, visible in Fig. 6, is that the effect of ϕ on skewness appears to be less pronounced at a higher Re number. While a largely non uniform skewness, at the lower Re number, underlines the distinct presence of DL-induced cusp structures which survive the effect of incident turbulence, a more uniform skewness distribution, occurring at a higher Re, is a symptom of turbulence being the dominating factor in determining the flame morphology, with DL structures thus playing a lesser role. In this context we note that the bulk Re is linearly related to the turbulent Reynolds number, based on the integral scale, and thus to the turbulence intensity [37]. Extrapolating this concept to higher Re numbers, we should ultimately expect little or no effect of ϕ on skewness and thus on flame morphology, a fact that hints at the existence of an additional regime in which turbulence is the sole dominating factor irrespective of the presence of underlying DL instability whose effects are therefore partially or completely shadowed. The existence of this additional third regime of propagation was also observed experimentally by Al-Shahrany et al. [12], numerically in [19] and was conjectured by Chaudhuri et al. in [20]. Further evidence was found by Kobayashi et al. [10] who noted that the flame's fractal dimension is sensitive to pressure increase, responsible for triggering DL instabilities, only at low turbulence intensity whereas at higher intensity fractal dimension plateaus to a universal value irrespective of DL effects.

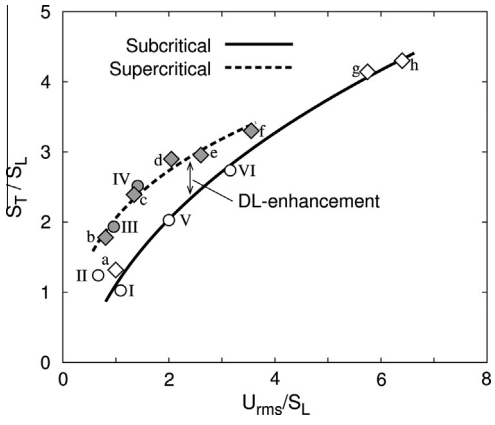

Fig. 7. Normalized turbulent propagation speed as a function of normalized turbulence intensity. Circles: $Re = 2500$, diamonds: $Re = 5000$ (experimental points labels correspond to Fig. 4 nomenclature).

We now proceed to analyze flame behavior in terms of turbulent flame speed as a function of turbulence intensity. Results are shown in Fig. 7 where we observe that the normalized turbulent flame speed data are best fitted by two distinct scaling laws, within the range of Re numbers under investigation. In particular, the concurrent analysis of Fig. 6 and Fig. 7 shows that flames conjectured to be supercritical, owing to highly skewed curvatures and near stoichiometric compositions, populate the scaling law associated to faster turbulent speeds (filled symbols, dashed line), which is thus named 'supercritical'. In other words, the turbulent flame speed is enhanced by the presence of DL instability (DL-enhancement) which, as we have seen, induces a characteristic morphology to the flame surface in terms of sharp, cusp-like structures. It can therefore be argued that such corrugation, which can be thought of as an additive effect to the turbulent wrinkling, is responsible for a systematic increase in flame area per unit flame-brush length which is in turn the cause for the enhancement in S_T/S_L. Subcritical flames, on the other hand, are deprived of the additional DL-driven corrugation mechanism and for this reason are observed to follow a different scaling law for S_T/S_L. Figure 7 also seems to reveal that the DL-enhancement decreases with turbulence intensity until it is completely depleted beyond some intensity threshold, thus leaving a single scaling law for S_T/S_L at higher intensity. Although additional data at higher Re would be needed to corroborate the latter statement, this would substantiate the existence of a third unique turbulence-driven regime of propagation, independent of DL effects as observed in [19,20].

The foregoing scenario thus furnishes experimental evidence for the existence of a dual mode of propagation for weakly turbulent premixed flames which was observed numerically in [18,19] and conjectured by Chaudhuri et al. in [20]. In particular, in this latter study, the existence of a DL-enhanced turbulent propagation regime is subject to the condition that, given a flame perturbation wavenumber k, its linear growth rate ω, given by the dispersion relation, be greater than the characteristic eddy frequency $\omega_{\text{turb}} = 2\pi/\tau_{\text{turb}}$ where τ_{turb} is the eddy turnover time estimated as the ratio of turbulent kinetic energy to mean dissipation rate. Defining the non dimensional parameter $\beta = \omega_{\text{turb}}/\omega$ for all scales smaller than the integral length scale, then the region $\beta < 1$ indicates that a DL instability can indeed develop in a turbulent environment and thus a supercritical propagation mode can exist. Figure 8 shows the locus $\beta = 1$, estimated following [20] for a $\phi = 1$ propane–air mixture, within a turbulent combustion diagram populated by the experimental points of the present study. We note that supercritical flames (shown with filled symbols)

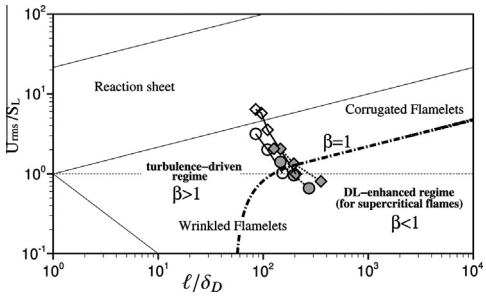

Fig. 8. Modified premixed turbulent combustion diagram with superimposed experimental points. Dash–dot curve is the $\beta = 1$ locus (calculated at $\phi = 1$); Circles: $Re = 2500$; Diamonds: $Re = 5000$; Filled/empty symbols refer to super/subcritical scaling laws in Fig. 7.

have the tendency to fall within the $\beta < 1$ region thus confirming the validity of the conjectured criterion defining the DL-enhanced regime.

Fits of the kind $S_T/S_L \sim (U_{rms}/S_L)^n$ can be sought for the scaling laws of Fig. 7. We find for the subcritical propagation mode a scaling exponent $n_{sub} \approx 0.4$ which confirms previous experimental studies [9] and is close to the analytical expression proposed in [20] where $n_{sub} = 0.5$. For the supercritical propagation mode we find $n_{sup} \approx 0.25$ which is substantially smaller than n_{sub}. This indicates that the DL-induced structures of the supercritical case appear to be less sensitive to turbulence in spite of the fact that their higher corrugation causes an enhancement of turbulent flame speed. This property of supercritical flames was repeatedly observed in [18,19,16] using different numerical approaches and where it was termed 'resilience' to the incident turbulence.

6. Conclusions

An experimental investigation of Darrieus–Landau (DL) hydrodynamic instability effects on turbulent premixed flame propagation was performed using propane–air Bunsen flames at atmospheric pressure. Measurements of turbulent flame speed and flame curvature statistics were carried out. Two distinct scaling laws were observed for the turbulent flame speed as a function of turbulence intensity. A law exhibiting higher turbulent flame speed is observed for flames closer to stoichiometric composition and possessing enhanced negative skewness of curvature p.d.f.'s. Flames with such characteristics are shown to be more likely to exhibit typical DL instability effects in terms of cusp-like corrugation. Super- and subcritical modes of propagation can thus defined, respectively based on the presence or absence of such effects. Increased flame corrugation is therefore conjectured to cause a DL-induced enhancement of the turbulent flame speed in the supercritical mode which is absent in the subcritical mode. The morphological features of the two modes of propagation were also investigated and observed by means of direct numerical simulations of methane–air Bunsen flames, confirming the presence of DL cusp-like corrugation in the supercritical case, introducing sharp negative bursts in flame curvature.

Power law fits $S_T/S_L \sim (U_{rms}/S_L)^{n_{sub,sup}}$ reveal $n_{sub} < n_{sub} \approx 0.4$ which confirm previous numerical [16,19] and analytical [20] studies. Results also suggest that at higher intensity, turbulence is the prevailing phenomenon, shadowing any DL-driven effects and therefore unifying the dual propagation mode into a single turbulence-driven mode. In a future study, additional data will be gathered to corroborate the existence of such turbulence-driven mode.

Acknowledgments

F. Creta is grateful to Dr. H.N. Najm for his valuable comments and scientific feedback and for providing precious assistance with the dflame code.

References

[1] D. Bradley, M. Lawes, M. Mansour, *Flow Turbul. Combust.* 87 (2011) 191–204.
[2] S. Filatyev, J. Driscoll, C. Carter, J. Donbar, *Combust. Flame* 141 (2005) 1–21.
[3] J. Driscoll, *Progr. Energy Combust. Sci.* 34 (2008) 91–134.
[4] P. Cambray, G. Joulin, *Proc. Combust. Inst.* 24 (1992) 61–67.
[5] V. Bychkov, *Phys. Rev. E* 68 (2003) 663041–6630412.
[6] V. Akkerman, V. Bychkov, *Combust. Theory Model.* 9 (2005) 323–351.
[7] H. Kobayashi, T. Tamura, K. Maruta, T. Niioka, *Proc. Combust. Inst.* 26 (1996) 389–396.
[8] R. Paul, K. Bray, *Proc. Combust. Inst.* 26 (1996) 259–266.
[9] H. Kobayashi, Y. Kawabata, K. Maruta, *Proc. Combust. Inst.* 27 (1998) 941–948.
[10] H. Kobayashi, H. Kawazoe, *Proc. Combust. Inst.* 28 (2000) 375–381.
[11] V. Savarianandam, C. Lawn, *Combust. Flame* 146 (2006) 1–18.
[12] A. Al. Shahrany, D. Bradley, M. Lawes, K. Liu, R. Woolley, *Combust. Sci. Technol.* 178 (2006) 1771–1802.
[13] D. Bradley, M. Lawes, L. Kexin, M. Mansour, *Proc. Combust. Inst.* 34 (2013) 1519–1526.
[14] F. Creta, M. Matalon, *Proc. Combust. Inst.* 33 (2011) 1087–1094.
[15] C. Clanet, G. Searby, *Phys. Rev. Lett.* 80 (1998) 3867–3870.
[16] M. Matalon, F. Creta, *Comptes Rendus Mecanique* 340 (2012) 845–858.

[17] N. Fogla, F. Creta, M. Matalon, *Proc. Combust. Inst.* 34 (2013) 1509–1517.
[18] F. Creta, M. Matalon, *J. Fluid Mech.* 680 (2011) 225–264.
[19] F. Creta, N. Fogla, M. Matalon, *Combust. Theory Model.* 15 (2011) 267–298.
[20] S. Chaudhuri, V. Akkerman, C. Law, *Phys. Rev. E* 84 (2011).
[21] P. Pelce, P. Clavin, *J. Fluid Mech.* 124 (1982) 219–237.
[22] M. Matalon, B. Matkowsky, *J. Fluid Mech.* 128 (1982) 239–259.
[23] P. Clavin, *Progr. Energy Combust. Sci.* 11 (1985) 1–59.
[24] M. Matalon, C. Cui, J. Bechtold, *J. Fluid Mech.* 487 (2003) 179–210.
[25] J. Bechtold, Matalon, *Combust. Flame* 127 (2001) 1906–1913.
[26] L.K. Tseng, M.A. Ismail, G.M. Faeth, *Combust. Flame* 95 (1993) 410–426.
[27] R. Petersen, H. Emmons, *Phys. Fluids* 4 (1961) 456–464.
[28] H. Najm, P. Wyckoff, O. Knio, *J. Comput. Phys.* 143 (1998) 381–402.
[29] O. Knio, H. Najm, P. Wyckoff, *J. Comput. Phys.* 154 (1999) 428–467.
[30] H. Najm, O. Knio, *J. Sci. Comp.* 25 (2005) 263–287.
[31] M. Valorani, F. Creta, D. Goussis, J. Lee, H. Najm, *Combust. Flame* 146 (2006) 29–51.
[32] F. Battista, F. Picano, G. Troiani, C.M. Casciola, *Phys. Fluids* 23 (2011) 123304.
[33] F. Picano, F. Battista, G. Troiani, C.M. Casciola, *Exp. Fluids* 50 (2011) 75–88.
[34] G. Troiani, M. Marrocco, S. Giammartini, C.M. Casciola, *Combust. Flame* 156 (2009) 608–620.
[35] G. Troiani, *Combust. Flame* 156 (2009) 539–542.
[36] S. Pfadler, F. Beyrau, A. Leipertz, *Opt. Expr.* 15 (2007) 15444–15456.
[37] S. Pope, *Turbulent Flows*, 1st ed., Cambridge University Press, Cambridge, UK, 2000.
[38] G. Troiani, F. Battista, F. Picano, *Combust. Flame* 160 (2013) 2029–2037.